Neuron
Article

Attentional Modulation of Cell-Class-Specific Gamma-Band Synchronization in Awake Monkey Area V4

Martin Vinck,[1,2,3,7,*] Thilo Womelsdorf,[2,4,7] Elizabeth A. Buffalo,[5] Robert Desimone,[6] and Pascal Fries[1,2,*]
[1]Ernst Strüngmann Institute (ESI) for Neuroscience in Cooperation with Max Planck Society, 60528 Frankfurt am Main, Germany
[2]Donders Centre for Brain, Cognition, and Behaviour, Radboud University Nijmegen, 6525 EN Nijmegen, The Netherlands
[3]Center for Neuroscience, Swammerdam Institute for Life Sciences, University of Amsterdam, 1098 XH Amsterdam, The Netherlands
[4]Department of Biology, Centre for Vision Research, York University, Toronto, Ontario M6J 1P3, Canada
[5]Department of Physiology and Biophysics, University of Washington School of Medicine, and the Washington National Primate Research Center, Seattle, WA 98195, USA
[6]McGovern Institute for Brain Research at MIT, Cambridge, MA 02139, USA
[7]These authors contributed equally to this work
*Correspondence: martinvinck@gmail.com (M.V.), pascal.fries@esi-frankfurt.de (P.F.)
http://dx.doi.org/10.1016/j.neuron.2013.08.019

SUMMARY

Selective visual attention is subserved by selective neuronal synchronization, entailing precise orchestration among excitatory and inhibitory cells. We tentatively identified these as broad (BS) and narrow spiking (NS) cells and analyzed their synchronization to the local field potential in two macaque monkeys performing a selective visual attention task. Across cells, gamma phases scattered widely but were unaffected by stimulation or attention. During stimulation, NS cells lagged BS cells on average by ~60° and gamma synchronized twice as strongly. Attention enhanced and reduced the gamma locking of strongly and weakly activated cells, respectively. During a prestimulus attentional cue period, BS cells showed weak gamma synchronization, while NS cells gamma-synchronized as strongly as with visual stimulation. These analyses reveal the cell-type-specific dynamics of the gamma cycle in macaque visual cortex and suggest that attention affects neurons differentially depending on cell type and activation level.

INTRODUCTION

Selective visual attention modulates neuronal synchronization within and between visual areas (Bosman et al., 2012; Buschman and Miller, 2007; Fries et al., 2001b; Gregoriou et al., 2009). Neuronal synchronization is brought about by an interplay between excitatory and inhibitory cells (Buzsáki and Wang, 2012). Yet, the differential synchronization of these two cells classes has not yet been studied in the awake monkey visual cortex during well-controlled selective visual attention. We take the first steps in this direction by classifying cells based on their average waveform and analyzing the different cell classes' alpha and gamma local field potential (LFP) locking and their modulation by selective attention.

Selective attention enhances gamma-band synchronization among neurons activated by the attended stimulus in areas V4 (Chalk et al., 2010; Fries et al., 2001b) and V2 (Buffalo et al., 2011), and it either reduces (Chalk et al., 2010) or enhances (Buffalo et al., 2011) gamma-band synchronization in area V1. The attentional effects on V4 gamma-band synchronization are predictive of attentional reaction time benefits (Womelsdorf et al., 2006). When two stimuli activate separate groups of V1 neurons with different gamma rhythms, only the rhythm induced by the attended stimulus synchronizes to V4, most likely mediating the selective interareal communication of attended stimulus information (Bosman et al., 2012; Grothe et al., 2012).

Gamma-band synchronization within a local neuronal group is governed by the interneuron network and its interaction with activated excitatory neurons (Börgers and Kopell, 2005; Buzsáki and Wang, 2012; Cardin et al., 2009; Cobb et al., 1995; Sohal et al., 2009; Tiesinga and Sejnowski, 2009; Whittington et al., 1995). These mechanistic insights have been captured in two models: the interneuron network gamma (ING) and the pyramidal cell interneuron network gamma (PING) models of gamma-band synchronization. While in both, the inhibitory interneurons play a dominant role in generating the gamma rhythm, ING models (Whittington et al., 1995; Wang and Buzsáki, 1996; Bartos et al., 2007) have the pyramidal cells simply entrained, while PING models lend them a role in sustaining the rhythm after they are entrained (Börgers and Kopell, 2005; Eeckman and Freeman, 1990; Leung, 1982; Wilson and Cowan, 1972). PING models suggest that within the gamma cycle, pyramidal cells fire first and trigger the firing of inhibitory interneurons, leading to a characteristic average phase relation. This phase relationship is thought to be critical for the maintenance of gamma-band synchronization and has been confirmed in recordings from rat hippocampus (Csicsvari et al., 2003; Tukker et al., 2007) and anesthetized ferret frontal cortex (Hasenstaub et al., 2005), but not yet in monkey visual cortex, a prime model to study the putative role(s) of gamma-band synchronization. In awake monkey visual cortex, we can separate the effects of visual stimulation and attentional top-down control on the synchronization of putative pyramidal cells and inhibitory interneurons.

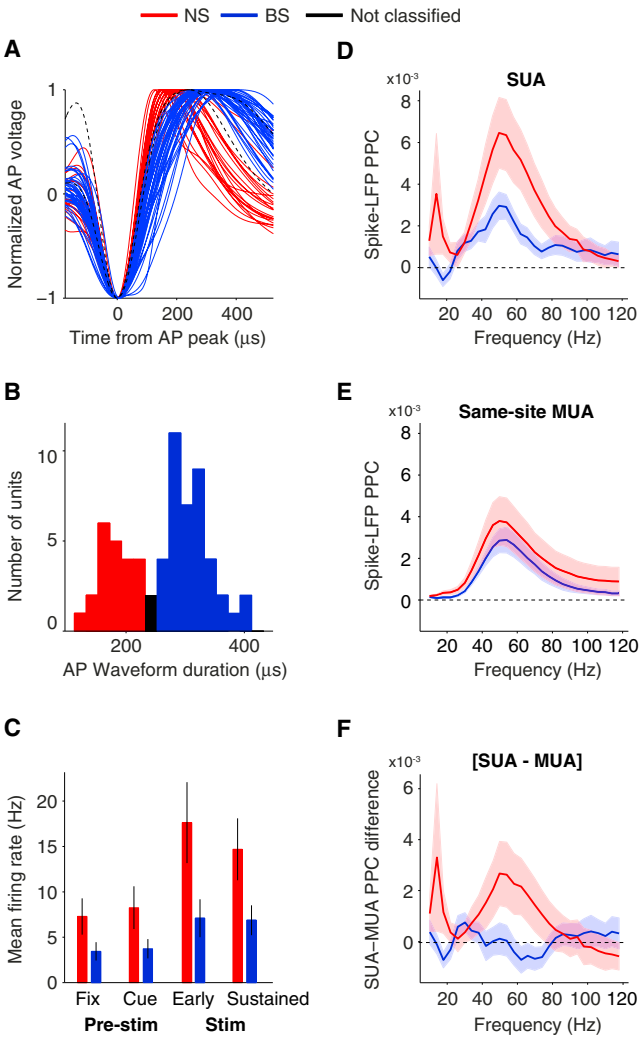

Figure 1. Classification of NS and BS Cells Based on AP Waveforms and Their Differences in Gamma Locking during Visual Stimulation

(A) Normalized voltage versus time from AP peak for all average waveforms of the isolated single units.

(B) Histogram of AP peak-to-trough durations.

(C) Average firing rate for different task periods (vertical lines indicate SEM). Left-to-right: prestimulus fixation, cue, early onset (0–0.3 s after grating stimulus onset), and sustained stimulus period.

(D) Average spike-LFP PPC spectra. Shadings indicate SEM.

(E) Average PPC for the same-site MUAs corresponding to either the NS or BS cells. Shadings indicate SEM.

(F) Average SUA-MUA PPC difference [$PPC_{SUA} - PPC_{MUA}$] versus frequency. Shadings indicate SEM.

See also Figures S1 and S2.

Pyramidal cells and inhibitory interneurons can be tentatively separated in recordings from awake behaving monkeys by sorting spikes according to their waveform (e.g., Mitchell et al., 2007). Distributions of spike waveform across populations of neurons often have a characteristic bimodal shape, with broad spiking (BS) and narrow spiking (NS) cells typically labeled as putative pyramidal neurons and putative inhibitory interneurons, respectively. We have applied this approach to data from simultaneous recordings of single unit activity (SUA), multiunit activity (MUA), and LFP from four nearby electrodes in area V4 of two monkeys performing a selective visual attention task.

RESULTS

Identification of NS and BS cells

We recorded spiking activity of 64 isolated single units from area V4 in two awake macaque monkeys (M1 and M2). For each neuron, we normalized the average action potential (AP) waveform by dividing by its peak-to-trough amplitude. We then aligned the average AP waveforms' peaks (Figure 1A). The distribution of AP peak-to-trough durations was bimodal (Figure 1B; $p < 0.05$, Hartigan's dip test), as in a previous V4 study (Mitchell et al., 2007). Neurons were classified as either NS or BS if their average AP's peak-to-trough duration was smaller than 230 ms (n = 22) or larger than 260 ms (n = 40), respectively. NS cells had higher mean firing rates than BS cells in both the prestimulus and stimulus period (Figure 1C; randomization test, $p < 0.05$). In the autocorrelogram, BS cells had earlier median peak times than NS cells at respectively 4 ± 0.63 (±SEM) versus 22 ± 4.88 ms ($p < 0.001$, Mann-Whitney U test, n = 62). In the interspike interval (ISI) distribution, BS and NS cells showed median peak times of 5 ± 1.38 and 12 ± 3.5 ms, respectively ($p < 0.05$, Mann-Whitney U test, n = 62). BS cells showed relatively bursty firing patterns, with local variation (LV) (Shinomoto et al., 2009) values significantly higher than one (median 1.58 ± 0.07, $p < 0.001$, rank Wilcoxon test) and higher than those of NS cells (median 1.02 ± 0.19, $p < 0.001$, Mann-Whitney U test, n = 62). The observed differences in ISI, autocorrelation peak times and burstiness during sustained visual stimulation are in good agreement with findings from the rodent hippocampus (Csicsvari et al., 1999). Overall, these differences in waveform and spike train statistics suggest that our sample of NS cells mostly contained inhibitory interneurons, while our sample of BS cells mostly contained pyramidal cells (Barthó et al., 2004; Csicsvari et al., 1999; Hasenstaub et al., 2005; McCormick et al., 1985; Mitchell et al., 2007; Nowak et al., 2003).

Precision of Phase Locking in Sustained Stimulation Period

We related spikes from isolated single units to the average LFP recorded simultaneously from up to four separate electrodes spaced at a fixed horizontal distance of 650–900 μm and a median vertical distance of 298 μm (with lower and upper quartiles of 144 and 585 μm). We quantified the precision of spike-LFP phase locking by using the spike-LFP pairwise phase consistency (PPC), a metric unbiased by spike rate or count (Vinck et al., 2012, 2010b). During the sustained visual stimulation period (>0.3 s after the onset of the stimulus grating, lasting until the first target or distracter change), spikes were strongly locked to LFP gamma-band oscillations (~50 Hz; Figure 1D), consistent with Fries et al. (2001b, 2008). Henceforth, we will investigate this gamma locking in more detail and report locking statistics for the 50 Hz bin, which approximately encompasses the 30–70 Hz interval due to spectral smoothing (see Supplemental Experimental Procedures).

We found that gamma PPCs were almost twice as high for NS than BS cells (Figure 1D; $p < 0.01$, randomization test, $N_{NS} = 22$, $N_{BS} = 39$ for Figures 1D–1F; for monkeys M1 and M2 see Figures S1A, S1B, S2A, and S2B available online). The use of the PPC ensures that this difference is neither confounded by spike rate nor count. Irrespective of this, there might still be a physiological difference in locking strength between strongly and weakly firing units. To test whether the difference in gamma locking between NS and BS cells is due to such a physiological difference, we eliminated weakly firing BS cells until the mean firing rate was matched between BS and NS cells. After this rate stratification, NS cells still showed a stronger gamma locking than BS cells (BS: [mean PPC for high rate] = $3.1 \times 10^{-3} \pm 1.1 \times 10^{-3}$, $p < 0.05$, randomization test, $N_{BS} = 17$). Also, gamma PPC values were not correlated with AP waveform peak-to-trough duration (NS: Spearman $\rho = -0.086$, $p = 0.7$; BS: $\rho = -0.16$, $p = 0.31$), consistent with the notion that the separation based on waveform provided a separation into actual classes.

Several factors influence the gamma locking of spikes. One important known factor is the precise cortical layer (Buffalo et al., 2011), yet many other factors like the state of the animal might play a role. These factors might, in principle, be confounded with the probability of recording a BS versus an NS cell. And, even if they are not confounded, our limited sample size might lead to insufficient averaging-out of those factors. In order to assess the overall locking strength for a given recording site (and time, state, etc.), independent of the BS or NS characteristics of the recorded single unit, we analyzed the unsorted MUAs that were recorded from the same electrodes as the isolated units under consideration, while excluding the isolated single unit from the corresponding MUA. Based on the firing rates of MUA versus single units, we estimate that a typical MUA contained 10 to 20 single units, thereby providing a reasonable local average. Henceforth, we refer to these unsorted MUAs with the SUA excluded as the same-site MUAs. Same-site MUA PPCs did not differ between sites delivering isolated NS versus BS units (Figure 1E) (not significant [n.s.], bootstrap test). This suggests that the overall gamma locking did not differ between the recording locations of BS and NS cells. Please note that if the MUA from a BS or NS recording site had been biased to contain more BS or NS cells, this would have created similar differences for the same-site MUA as for the respective SUA analysis, which we did not find. Although the same-site MUA PPC did not differ between NS and BS cells, it is conceivable that same-site MUA PPC varied across sites. In order to eliminate the variability in PPCs across units that is caused by differences in recording location, we computed, for each unit separately, the SUA-MUA PPC difference. This measure is defined as the difference between a SUA's PPC and its corresponding same-site MUA's PPC [$PPC_{SUA} - PPC_{MUA}$], such that a value >0 indicates stronger spike-LFP locking for the SUA than its corresponding same-site MUA. SUA-MUA gamma PPC difference was higher for NS than BS cells ($p < 0.05$, randomization test) and significantly different from zero only for NS cells ($p < 0.05$, bootstrap test) (Figure 1F). Hence, it is unlikely that the observed difference in gamma PPC between NS and BS cells (Figure 1D) was caused by differences in recording locations.

In neocortex, there are more BS than NS cells (Figure 1B, Mitchell et al. (2007)). However, NS cells have higher firing rates, such that the MUA may contain approximately equal proportions of NS and BS spikes. Based on these estimates, the MUA-LFP PPC is expected to attain PPC values in between the BS and NS cells' PPC. In addition, we will demonstrate below that BS and NS cells lock on average to different gamma phases and that individual single units often lock to widely varying gamma phases. Assuming that our MUAs typically contained both BS and NS cells and individual cells that cover at least a small part of the overall intercell phase variance, this predicts that the MUA-LFP PPC is substantially smaller than the average PPC of its constituent SUAs, consistent with our observations.

Precision of Phase Locking in Prestimulus Period

We found that NS cells were more gamma locked than BS cells during the sustained visual stimulation period. NS cells might also be more gamma locked than BS cells during network states in which cells receive only weak excitatory drive. Previous studies have shown that MUA-LFP gamma locking and LFP gamma power are weak in the absence of visual stimulation or in the presence of low-contrast visual stimuli in the RF (receptive field) (Fries et al., 2008; Henrie and Shapley, 2005; Ray and Maunsell, 2010), although Fries et al. (2008) and Engel et al. (2001) have shown that MUA-LFP gamma locking can be reliably detected in the prestimulus period of the current task.

We analyzed the prestimulus period separately for the fixation (Figures 2A and 2B) and the cue period (Figures 2C and 2D; Figures 2E and 2F show both periods together for the lower frequencies). The fixation period started when the monkey had grasped the response bar and continued for >750 ms, ending with the appearance of the attentional cue. A cue period followed, lasting until the onset of a stimulus grating in the recorded neurons' RFs (and the simultaneous onset of a grating outside the RF). BS cells exhibited much lower gamma PPCs in the fixation (mean ± SEM of [$PPC_{stim} - PPC_{fix}$] = $4.3 \times 10^{-3} \pm 1.0 \times 10^{-3}$; $p < 0.001$, bootstrap test, $n = 33$) and the cue period ($2.8 \times 10^{-3} \pm 0.7 \times 10^{-3}$, $p < 0.001$, $n = 33$) than in the sustained stimulation period (Figures 2A and 2C). A potential concern is that prestimulus PPC may have been particularly variable because of low spike counts. To increase the relative contribution of cells with high spike counts, we computed weighted PPC group averages, with the relative contribution of a unit proportional to its spike count (Figures 2B and 2D; see also Supplemental Experimental Procedures). This analysis demonstrated that the relatively low BS cells' gamma PPC values did not arise because of low spike counts, yet it did reveal a shallow bump in the PPC spectrum at gamma frequencies.

The weak gamma locking of BS cells during the fixation and cue period contrasted sharply with the degree of gamma locking in NS cells. During the cue period, NS cells exhibited much stronger gamma locking than BS cells ($p < 0.01$, randomization test; Figure 2C), with NS gamma PPCs reaching levels similar to the sustained stimulation period (Figure 2C, mean of [$PPC_{stim} - PPC_{cue}$] = $0.61 \times 10^{-3} \pm 2.3 \times 10^{-3}$, $n = 17$, n.s., bootstrap test). This observation held true when PPC averaging was weighted by firing rates (Figure 2D). This state of strong NS gamma locking in the cue period occurred despite much lower firing rates than in the stimulus period (Figure 1C). NS cells' gamma PPCs were much higher in the cue (Figure 2C) than in the fixation period (Figure 2A;

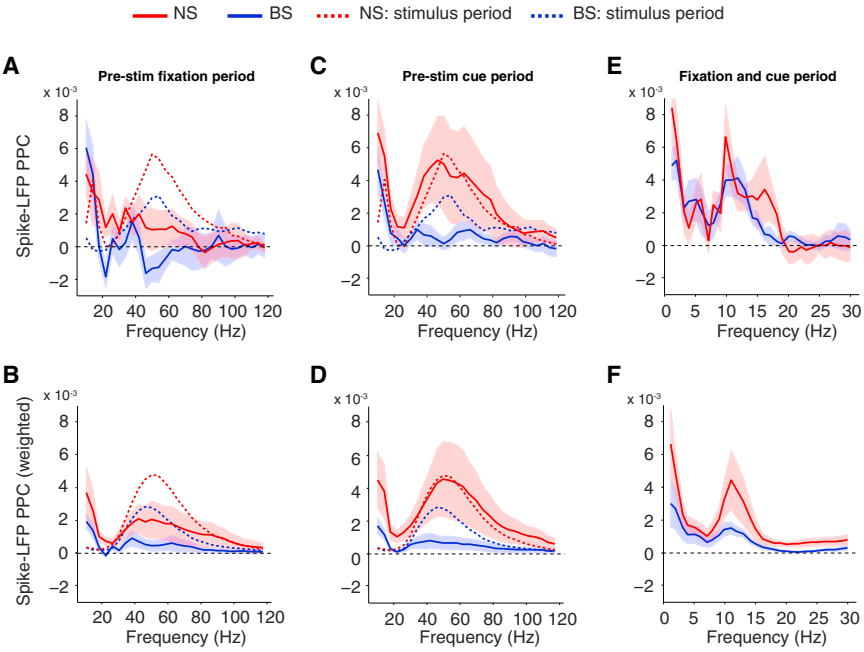

Figure 2. Precision of Prestimulus Phase Locking

(A) Average spike-LFP PPC spectra for the prestimulus fixation period. Dashed lines indicate average PPC for sustained stimulus period. Shadings indicate SEM.

(B) Same as (A), but now shown the weighted PPC group average, with the relative weight of a unit proportional to its spike count. Shadings indicate SEM.

(C) Same as (A), but now for the cue period. Shadings indicate SEM.

(D) Same as (B), but now for cue period. Shadings indicate SEM.

(E) Same as (A) and (C), but now for the complete prestimulus period (fixation onset to stimulus onset) and low frequencies. Shadings indicate SEM.

(F) Same as (B) and (D), but now for complete prestimulus period and low frequencies. Shadings indicate SEM.

See also Figures S1, S3, and S4.

$[PPC_{cue} - PPC_{fix}] = 4.0 \times 10^{-3} \pm 2.1 \times 10^{-3}$, $p < 0.01$, bootstrap test, $n = 15$), and this difference in NS cells' gamma PPCs occurred again in the absence of significant differences in firing rate between the fixation and cue period (Figure 1C; NS: $p = 0.27$ and $p = 0.37$ for rank Wilcoxon test on $[FR_{cue} - FR_{fix}]$ and $[(FR_{cue} - FR_{fix})/(FR_{cue} + FR_{fix})]$; BS: $p = 0.53$ and $p = 0.38$ for same tests). Moreover, we did not find a correlation between a given NS cell's gamma PPC value in the cue period, and its firing rate in the cue period relative to the fixation period $[FR_{cue}/FR_{fix}]$ ($p = 0.53$, Spearman regression, $n = 15$).

For some units ($n = 9$), attention was cued using a block design, i.e., without an "uncued" fixation period available. After inclusion of these units, we still found higher gamma PPC values for NS ($[PPC_{stim} - PPC_{cue}] = 2.0 \times 10^{-3} \pm 2.3 \times 10^{-3}$, $n = 21$, n.s., bootstrap test) than BS cells ($[PPC_{stim} - PPC_{cue}] = 2.7 \times 10^{-3} \pm 0.97 \times 10^{-3}$, $p < 0.01$, $n = 37$) in the cue period (Figures 3A and 3B; $p < 0.05$, randomization test; for monkeys M1 and M2 see Figures S1A, S1B, and S3A–S3D). Hence, we included these units for further cue period analyses.

To exclude the possibility that NS cells were recorded from sites where overall prestimulus spiking activity was more gamma locked, we computed the same-site MUA's PPC and the SUA-MUA PPC difference. For recording sites delivering NS cells, cue period same-site MUA gamma PPCs ($0.99 \times 10^{-3} \pm 0.32 \times 10^{-3}$) were much smaller than NS gamma PPCs (Figures 3C–3E; $p < 0.05$, bootstrap test, $n = 21$). Same-site MUA gamma PPCs did not differ between sites corresponding to NS and BS units (Figure 3C; n.s., randomization test).

Analysis of the LFP revealed a clear peak in LFP-LFP phase-coupling in the gamma-band both in the fixation and cue period (Figure S4A), despite no visible gamma peak in the LFP power spectrum (Figure S4C). LFP-LFP coupling values (Figure S4B) and gamma LFP power (Figure S4D) were increased in the cue relative to the fixation period.

In sum, during the cue period, in the absence of a stimulus in the recorded neurons' RFs, while BS cells showed only weak gamma locking, NS cells showed much stronger gamma locking, similar to the level observed with visual stimulation inside their RFs. This finding suggests that strong NS gamma locking in the cue period was not a mere consequence of an increase in the strength and rhythmicity of bottom-up synaptic inputs, but that it resulted most likely from top-down control. Moreover, this finding suggests that V4 NS cells can maintain strong gamma locking in network states where excitatory drive is weak and the recurrent excitatory inputs are only weakly gamma-band modulated.

Correlations in Gamma Locking between Periods

We next asked whether it is the same group of cells that exhibits gamma locking in both the prestimulus and sustained stimulus period, i.e., whether a unit's tendency to gamma lock in the prestimulus period predicts its tendency to do so in the stimulus period. A given BS unit's gamma PPC in the cue period could not be predicted by either its gamma PPC in the fixation ($p = 0.36$, Spearman regression, $n = 33$) or stimulus period ($p = 0.96$, Spearman regression, $n = 37$), presumably because BS gamma locking was strongly dependent on external visual inputs in the RF. In contrast, we found that an NS unit's gamma PPC in the cue period predicted its gamma PPC in both the fixation (Spearman $\rho = 0.54$, $p < 0.05$, $n = 15$) and sustained stimulation period (Spearman $\rho = 0.58$, $p < 0.01$, $n = 21$), showing that an NS cell's tendency to gamma lock was, to some degree, independent of external visual inputs.

Prestimulus Alpha Locking and Its Relationship to Gamma Locking

In addition to the observed PPC gamma peak, a prominent alpha peak was visible in the prestimulus spike-LFP PPC spectrum

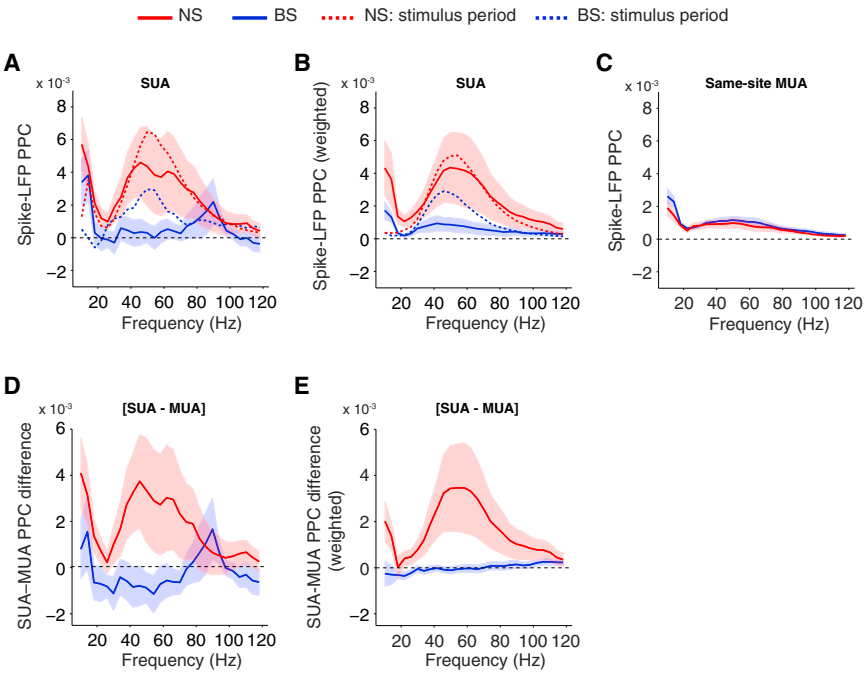

Figure 3. Comparison of MUA and SUA Phase Locking in the Prestimulus Cue Period

(A) Average spike-LFP PPC spectra for the prestimulus fixation period, including eight cells that were recorded with a block design, i.e., without an "uncued" fixation period. Dashed lines indicate average PPC for sustained stimulus period. Shadings indicate SEM.

(B) Same as (A), but now shown the weighted PPC group average. Shadings indicate SEM.

(C) Average spike-LFP PPC spectra for the same-site MUAs corresponding to either the NS or BS cells, in the cue period. Shadings indicate SEM.

(D) Average SUA-MUA PPC difference for the cue period. Shadings indicate SEM.

(E) Same as (D), but now shown the weighted average of the SUA-MUA PPC difference (similar to Figures 2B, 2D, and 2F). Shadings indicate SEM.

See also Figures S3 and S4.

(Figures 2E and 2F), in agreement with previous findings (Bollimunta et al., 2008; Fries et al., 2008). Henceforth, we report alpha locking statistics for the 10 Hz bin, which approximately encompasses the 7.5–12.5 Hz interval due to spectral smoothing (see Supplemental Experimental Procedures). No significant difference between NS and BS cell alpha PPC was observed for any prestimulus period (Figures 2A, 2C and 2E, n.s., randomization test), though the weighted PPC did differ significantly at 12 Hz when pooling fixation and cue period (Figure 2F).

For NS cells, gamma locking in the cue period coexisted with strong alpha locking, with many NS cells locking both to alpha and gamma LFP cycles in the prestimulus period (38.1% colocking of all NS cells, 52.3% at gamma, 62.0% at alpha, $p < 0.05$, Rayleigh test; $n = 21$), showing that the presence of locking in these two frequency bands was not mutually exclusive. The co-occurrence of alpha and gamma raises the question whether a unit's tendency to alpha lock predicts it propensity to gamma lock. We did not detect a significant correlation between alpha and gamma PPC across either NS ($p = 0.9$, Spearman regression, $n = 21$), or BS cells ($p = 0.53$, Spearman regression, $n = 37$) during the cue period. In sum, a given NS cell can participate in both gamma- and alpha-synchronization, such that superficial NS cells may play a role in integrating information processing occurring in these two frequency bands, which have different laminar profiles (Bollimunta et al., 2008; Buffalo et al., 2011). Furthermore, the degree to which a cell participates in one of these two rhythms can be independently regulated, consistent with the theories that appoint different mechanistic origins to both rhythms (Bollimunta et al., 2008; Lopes da Silva et al., 1973).

Phase of Gamma and Alpha Locking

In the prestimulus cue period, NS cells were gamma locked as much as during the stimulus period, while BS cells were hardly gamma locked (Figures 1D, 2C, and 3A). Thus, NS cells can maintain gamma-synchronization without significant recruitment of local BS cells into the gamma rhythm. This finding is consistent with ING models of gamma generation (Bartos et al., 2007; Wang and Buzsáki, 1996; Whittington et al., 1995). In PING models, both pyramidal cells and inhibitory interneurons are locked to the gamma rhythm, yet in a temporal sequence in which excitatory firing has a gamma phase lead over inhibitory firing (Börgers and Kopell, 2005; Eeckman and Freeman, 1990; Leung, 1982; Wilson and Cowan, 1972). During the stimulation period, both NS and BS cells were gamma locking (Figure 1D), allowing to test whether the precise timing differences between them abided by PING model predictions. Indeed, during sustained activation, NS cells fired on average at a later gamma phase (230.2 ± 54.9°, 95% confidence interval [CI], $n = 20$) than BS cells (170.4 ± 34.9°, $n = 33$) (Figure 4A; Figures S1C and S2C–S2D for the two monkeys separately), amounting to a gamma phase delay of 59.6° ($p < 0.05$, circular ANOVA). This phase delay did not disambiguate whether NS cells fired before or after BS cells in time. To understand this, we investigated the phase relation between NS and BS cells as a function of the frequencies ~50 Hz. If the phase relation increases approximately linearly with frequency, this corresponds to a fixed time lead of NS over BS cells, because a fixed time delay corresponds to increasing parts of the oscillation cycle when the cycle gets shorter for higher frequencies, i.e., at frequency f, phase delay ($\Delta\phi$) and time delay (Δt) are linearly related by $\Delta\phi = 2\pi f \Delta t$ (Nolte et al., 2008; Figure 6B in Phillips et al., 2013). The average gamma phase relation between NS and BS cells was indeed an increasing function of frequency (Figure 4B; Pearson $R = 0.975$, $p < 0.001$), suggesting that NS cells fired after BS cells in time. The phase delay of 59.6° therefore corresponds to a temporal delay of 3.3 ms.

In contrast, for prestimulus alpha locking (fixation and cue period combined to increase sensitivity), no significant difference was observed between the preferred firing phases of NS

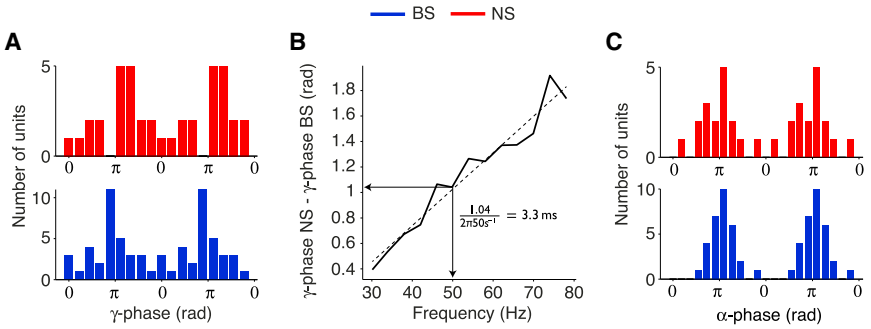

Figure 4. Differences in Locking Phase between NS and BS Cells

(A) Histogram of mean spike-LFP gamma phases across units. Only units for which the gamma PPC exceeded zero are shown.

(B) Mean gamma phase delay versus frequency. Dashed black line indicates linear regression fit (Pearson R = 0.93, $p < 0.001$).

(C) Histogram of preferred alpha phases in the complete prestimulus period (for units with an alpha PPC exceeding zero).

See also Figures S1 and S2.

(189.2 ± 35.7°, n = 19) and BS cells (197.6 ± 15.5°, n = 34, p = 0.61, circular ANOVA) (Figure 4C). We did not detect a systematic linear relationship between phase delay and frequency ~10 Hz.

Differences in the Preferred Phase of Locking among Neurons

The analysis above demonstrates that cells from different electrophysiological classes (NS or BS) tend to fire at different gamma phases. This finding raises the question whether neurons from the same cell class tend to fire at the same gamma phase, or whether systematic phase differences exist within the NS and BS cell classes. Figure 4A shows, per class, a distribution of preferred phases, and the dispersion in this distribution might be due either to a true variance of preferred phases, or merely to a noisy estimation of the preferred phase of each individual single unit. The latter is conceivable particularly for units with a limited number of spikes. In order to test directly whether units from the same cell class had different preferred phases, we compared all possible intracell class pairs of single units by means of a circular ANOVA (in this test, a low number of spikes would merely render the test insensitive). The circular ANOVA revealed that a substantial proportion of unit pairs from the same electrophysiological class indeed had a significantly different mean gamma phase (NS: 65.4% of 231 single unit pairs; BS: 44.8% of 741 single unit pairs; $p < 0.05$ for both tests). Note that the circular ANOVA has more statistical power for cells with higher spike counts and is hence unsuitable for comparisons between neuron types.

We were interested in directly measuring the degree to which neurons, recorded in different sessions, were synchronized in terms of their phase of spiking in the LFP gamma cycle, which was taken as a common clock across sessions. Using the LFP gamma cycle as a common clock allowed to indirectly measure phase synchronization between spike trains from single neurons that were not recorded at the same time. The PPC, for a single unit, measures to what extent different single spikes from the same neuron tend to cluster at the same phase, even though they are recorded in different trials. In analogy, we can measure to what extent spikes from a population of different neurons tend to cluster at the same phase, even though the neurons were (typically) recorded in different sessions. This defines a measure that we call network-PPC (Supplemental Experimental Procedures), which scales from 0 (no similarity) to 1 (full similarity) and is unbiased by spike count. If all neurons are synchronized with the same strength and same phase preference (i.e., identically distributed), then it is irrelevant whether a pair of spikes (and corresponding spike phases) is taken from the same or from two different neurons, and correspondingly the network-PPC will equal the average single unit PPC (as shown in Figure 1D). If a population of neurons has preferred gamma phases that are uniformly distributed over the gamma cycle, then the network-PPC is expected to be zero.

Two neurons may have very dissimilar phases, but may still be synchronized with a nonzero phase delay. These phase delays may well be corrected for by axonal delays, such that spikes can still arrive in phase at a postsynaptic target. We therefore also introduced a measure called the delay-adjusted network-PPC (Supplemental Experimental Procedures). This measure was constructed by first rotating the gamma phase distributions such that the two neurons' preferred phases were aligned. We then computed the similarity between the phases of the two neurons. This yielded, again, a pairwise consistency value between 0 and 1. If the two neurons have no reliable locking to the LFP gamma cycle, then the pairwise consistency value will be zero, if they are perfectly synchronized to the LFP gamma cycle, then the pairwise consistency will indicate that they are perfectly synchronized. Importantly, the delay-adjusted network-PPC provides an upper bound to the network-PPC. The delay-adjusted network-PPC quantifies the similarity among spike-LFP phases in the population of neurons as if all neurons had the same preferred phase relative to the LFP. Hence, the degree to which the network-PPC differed from the delay-adjusted network-PPC provides a measure of phase diversity in the population. Note that delay-corrected network-PPC has some positive sampling bias that is corrected for through bias subtraction (Supplemental Experimental Procedures).

We found that the delay-adjusted gamma network-PPC (NS: $5.1 \times 10^{-3} \pm 0.62 \times 10^{-3}$, n = 22; BS: $2.2 \times 10^{-3} \pm 0.43 \times 10^{-3}$, n = 39) and the mean single unit gamma PPC (Figure 1D) were an order of magnitude larger than the gamma network-PPC (Figure 5A; NS: $0.58 \times 10^{-3} \pm 0.23 \times 10^{-3}$; BS: $0.39 \times 10^{-3} \pm 0.19 \times 10^{-3}$, bootstrap test, $p < 0.001$, difference between NS and BS n.s.). Thus, while the majority of neurons fired reliably around their individual preferred gamma phase, we found that different neurons fired at strongly divergent preferred gamma phases. Further, NS cells are more synchronized individually to the LFP gamma cycle, yet do not fire more synchronously as a population than the BS cells.

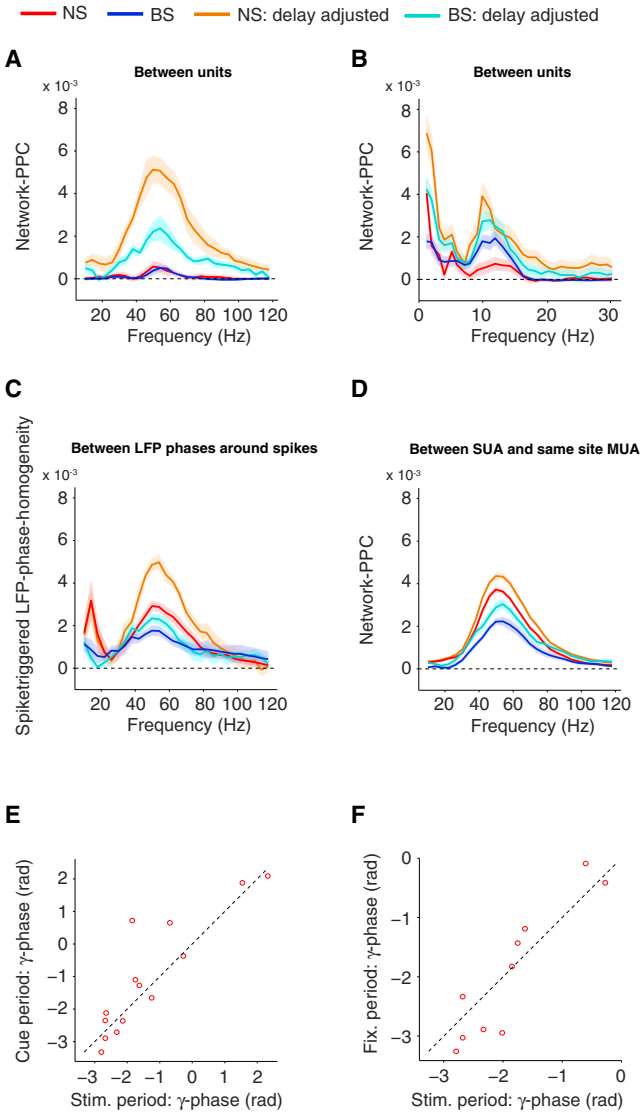

Figure 5. Diversity of Gamma Phases across Population

(A) Network-PPC versus frequency. The network-PPC indicates to what extent spikes from different neurons have similar phases. Shown in orange (NS) and cyan (BS) the delay-adjusted network-PPC that is obtained by setting the mean spike-LFP phase equal for all neurons. Shadings indicate SEM.

(B) Same as (A), but now for the low frequencies in the prestimulus period. Shadings indicate SEM.

(C) Same as (B), but now shown the spike-triggered LFP phase diversity, and its delay-adjusted version. The spike-triggered LFP phase diversity quantifies to what extent the distribution of spike-LFP phases measured relative to one (LFP) electrode is similar to the distribution of spike-LFP phases measured relative to another (LFP) electrode. Shadings indicate SEM.

(D) Same as (A) and (B), but now shown the network-PPC for same-site MUA and SUA. In this case, the network-PPC indicates to what extent the same-site MUA and the corresponding SUA have similar phases or not. Shadings indicate SEM.

(E) Mean gamma phase in stimulus period versus cue period, for NS cells with a spike-LFP PPC exceeding zero in both periods.

(F) Same as (E), but now for stimulus versus fixation period.

See also Figure S3.

This gamma phase diversity contrasted with the diversity in alpha phases. Figure 4C suggests that the distribution of BS cell prestimulus alpha phases is much less dispersed than the distribution of BS cell sustained stimulation gamma phases (Figure 4A), despite similar alpha and gamma locking strengths and higher spike counts (that de-noises the phase histograms) during the sustained stimulation period. Indeed, BS cells' alpha network-PPC was reduced by only ~35% ($2.1 \times 10^{-3} \pm 0.31 \times 10^{-3}$ versus $3.0 \times 10^{-3} \pm 0.48 \times 10^{-3}$, $p < 0.05$, bootstrap test, $n = 33$) relative to the delay-adjusted network-PPC, indicating that BS cells tended to fire at the same alpha phase (Figure 5B). While the BS cells' delay-adjusted network-PPC did not differ between the gamma and alpha frequency, the network-PPC was almost an order of magnitude larger for the alpha- than for the gamma-band ($0.54 \times 10^{-3} \pm 0.24 \times 10^{-3}$ versus $3.8.10^{-3} \pm 0.68$, $n = 18$, $p < 0.001$, bootstrap test). In other words, although BS cells are individually equally synchronized to the LFP gamma and alpha cycle, they fire more coherently as a population in the alpha-band. The high alpha network-PPC for BS cells contrasted with the low alpha network-PPC for NS cells, indicating a larger degree of alpha-phase differences between NS than between BS cells.

Diversity of LFP Phases around Spikes

One factor that may have contributed to the observed diversity in preferred gamma phases across units is variability in LFP phases across electrodes. To compare the diversity in LFP phases across electrodes with the diversity in preferred spike-LFP phases across single units, we defined a spike-LFP phase homogeneity measure (Supplemental Experimental Procedures), which assessed to what extent the spike phases relative to one LFP were coincident (in phase) with the spike phases relative to the other LFPs and is defined in analogy to the network-PPC. We then averaged these spike-LFP phase homogeneity values across single units and compared them to the delay-adjusted spike-LFP phase homogeneity values. We found little diversity of LFP phases in comparison to the homogeneity in spike-LFP phases across units, although the observed spike-LFP phase homogeneity was reduced by a factor of ~35%–40% relative to the delay-adjusted spike-LFP phase homogeneity (Figure 5C), consistent with Maris et al. (2013). We conclude that the diversity in LFP phases across electrodes was relatively low and thereby unlikely to contribute substantially to the observed diversity in spike-LFP phases across single units.

Dependence of Network-PPC on Spatial Distance

The diversity in preferred spike-LFP phases may be a function of spatial distances between units. A classic electrophysiological approach to examine whether a certain feature of the neural response has spatial structure is to test whether units recorded from the same electrode tend to behave more similarly than units recorded from separate electrodes. To test whether units from the same recording location fired at the same gamma phase or not, we computed the network-PPC between the SUAs and their corresponding same-site MUAs. Network-PPC was reduced only by a factor of ~15%–30% with respect to the delay-adjusted network-PPC (Figure 5D). This finding suggests that there is indeed considerable spatial structure in preferred SUA

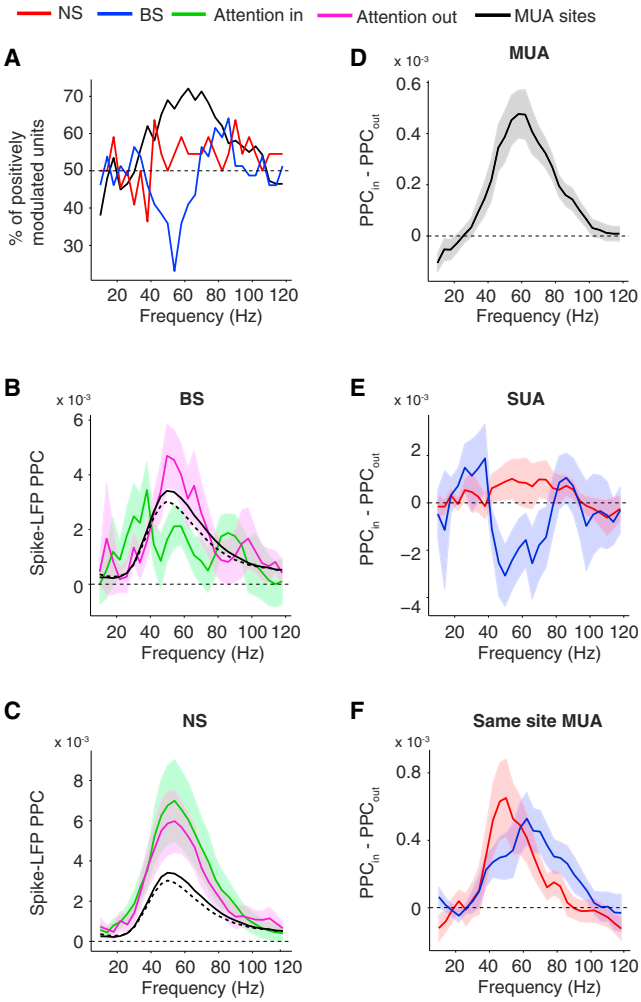

Figure 6. Effect of Attention on MUA-LFP and SUA-LFP PPC

(A) Percentage of SUAs (red, blue) and MUAs (black) for which the PPC was higher with attention inside than outside the RF.

(B) Average BS cell PPC versus frequency, separate for attention inside and outside the RF. Solid black and dashed black line correspond to MUA PPC with attention inside and outside the RF, respectively. Shadings indicate SEM.

(C) Same as (B), now for NS cells. Shadings indicate SEM.

(D) Frequency versus the average difference in MUA-LFP PPC between attention inside and outside the RF. Shadings indicate SEM.

(E) Same as (D), but now for NS and BS cells.

(F) Same as (E), but now for the same-site MUAs corresponding to either the NS (red) or BS (blue) cells. Shadings indicate SEM.

See also Figures S1 and S5.

spike-LFP gamma phases, such that nearby units fire approximately at the same preferred spike-LFP gamma phase. Considerable homogeneity between nearby units was also suggested by the above-mentioned finding that MUA gamma PPCs were not significantly different from BS cell gamma PPCs (Figures 1E, 1F, and 3C–3E), because a linear mixture of SUAs firing at different preferred LFP phases into one MUA should have resulted in a lower PPC than the average PPC of the individual SUAs. Nevertheless, circular ANOVA tests revealed a significant difference in preferred gamma phase between SUA and same-site MUA for a substantial number of sites for BS cells (41.0% of BS sites), as well as for NS cells (63.7% of NS sites).

In summary, our results indicate that the observed phase diversity within the same cell class has a major spatial component, since units from the same electrode tended to fire at approximately the same phase.

Relationship Gamma Phase between Periods

Given that the same NS cells tended to exhibit strong gamma locking in both the cue and sustained stimulus period, we asked whether NS cells tended to fire at the same gamma phase in the stimulus and prestimulus period. NS cells' mean gamma phases in the stimulus period were strongly correlated with their mean gamma phases both in the fixation (Pearson $R = 0.92$, $p < 0.001$, $n = 14$) and cue (Pearson $R = 0.88$, $p < 0.001$, $n = 10$) period (Figures 5E and 5F; see Figures S3E and S3F for monkeys M1 and M2). Thus, the reliable sequences of NS cell activations in the gamma cycle that occur during sustained visual stimulation are repeated in the absence of a visual stimulus in their RFs.

Effect of Selective Attention on Gamma Phase

We have previously shown that when visual stimulation with the preferred orientation induces higher firing rates, V1 spiking activity shifts to earlier gamma phases (Vinck et al., 2010a). Given the positive effect of attention on firing rates in the present task (Fries et al., 2008), we predicted that gamma phase may shift with selective attention. Yet, preferred gamma phases of firing during sustained simulation did not differ between attention inside and outside the RF, both for NS (mean [$phase_{in} - phase_{out}$] = $-5.16 \pm 13.9°$, 95% CI, $n = 21$) and BS cells ($-4.43 \pm 20.7°$, $n = 39$). Only a small and nonsignificant (binomial test, $p > 0.05$) fraction of neurons had a significant difference in preferred gamma phase between attention inside and outside the RF (BS: 10.3%, $n = 39$; NS: 9.5%, $n = 22$, $p < 0.05$, circular ANOVA).

Effect of Selective Attention on Firing Rate and Gamma Locking

Previous V4 studies have shown that selective attention to a single stimulus inside an RF increases not only firing rates, but also gamma-band LFP power, MUA-LFP and MUA-MUA gamma-band coherence (Fries et al., 2001b, 2008; Gregoriou et al., 2009). Indeed, we observed a significant average increase ($p < 0.001$, bootstrap test) in MUA-LFP gamma PPC, with the majority of MUAs ($p < 0.001$, binomial test, $n = 129$) having higher gamma PPCs with attention inside their RF (Figures 6A–6D). This effect was strongest at a higher gamma frequency (~60 Hz) than the observed 50 Hz peak in the SUA and MUA PPC spectrum (Figures 1D and 6B). Considering that the PPC is unbiased by spike count/rate and that the analyzed MUA data set was the same as in Fries et al. (2008), this result demonstrates unequivocally that the previously reported effect of selective attention on gamma-band synchronization (Fries et al., 2001b, 2008) was not confounded by its effect on firing rates.

We predicted that selective attention enhances gamma locking for isolated single units as well. Yet, we found an average decrease ($p < 0.05$, bootstrap test) in BS cells' gamma PPCs, with only a minority of units (at 54 Hz, 23%, $p < 0.05$, multiple-comparison-corrected binomial test, $n = 39$) having a higher

gamma PPC with attention inside their RF (Figures 6A, 6B, and 6E; see Figures S1D–S1F and S5 for monkeys M1 and M2). Selective attention had no detectable effect on the average NS cell gamma PPC (n.s., bootstrap test, n = 21), with approximately the same fraction of cells having a positive and negative PPC modulation with selective attention (Figures 6A, 6C, and 6E). To investigate whether the decrease in BS cell PPCs was also present in the other units recorded from the same electrodes, we examined the same-site MUA's PPC spectra. We found a significant increase in average gamma PPC for the same-site MUAs, both for same-site MUAs recorded from sites giving NS and BS cells (Figure 6F; $p < 0.05$, bootstrap test), without a significant difference to the attentional effect in PPC for all MUAs together.

The negative (BS) and neutral (NS) effects of selective attention on gamma-band synchronization stood in sharp contrast to the attentional effect on single unit firing rates, which were increased by an average of 11.8% ± 3.7% (68.8% of cells positively modulated, n = 64) with attention inside the RF, with no significant difference between NS (14.1% ± 7.5% increase, 68.2% of cells positively modulated, n = 22) and BS cells (11.1% ± 4.2% increase, 70.0% positively modulated, n = 40).

Relationships between Firing Rate, Gamma Locking, and Selective Attention

These findings raise the question why the positive modulation of MUA-LFP gamma PPC with selective attention was not mirrored in the SUA-LFP gamma PPC. A possible clue might be found in the fact that the average SUA-LFP PPC weights each SUA equally, because the PPC is estimated for each SUA separately (in a way that is independent of the firing rate) and then averaged across SUAs. By contrast, the MUA-LFP PPC implicitly weights each SUA that goes into the MUA mixture according to its firing rate: SUAs with higher firing rates will influence the MUA-PPC more than SUAs with lower firing rates. Consequently, the difference between the attentional effects on MUA and SUA PPC might be explained through one of the following scenarios or a combination of both: (1) with attention, SUAs with particularly high firing rate, and therefore particularly strong MUA contribution, might increase their gamma locking particularly strongly, and (2) with attention, SUAs with particularly strong gamma locking might increase their firing rates particularly strongly and thereby contribute more to the MUAs. In both cases, the correlation between rates and gamma locking should increase with attention.

To test this prediction, we calculated the Spearman rank correlation across SUAs, between the SUA rates and the PPC, and separately for the two attention conditions and show their difference between attention conditions in Figure 7A. We found that our prediction held, selectively in the gamma-band (NS and BS, $p < 0.05$ and $p < 0.01$ respectively, bootstrap test). In fact, PPC-rate correlations were significantly greater than zero when attention was inside the neurons' RF (NS: Spearman $\rho = 0.50$, $p < 0.001$; BS: 0.62, $p < 0.001$; $N_{NS} = 21$, $N_{BS} = 39$ for Figure 7; see Figures S1G–S1J and S6 for monkey M1 and Figures S1G–S1J and S7 for monkey M2), but not when it was outside the RF (NS: −0.07, n.s.; BS: −0.02, n.s.).

This analysis was done on the absolute SUA firing rates during sustained activation, which is a function of both baseline firing rate (defined here from fixation onset to stimulus onset), and the change in firing rate during visual stimulation relative to baseline. To investigate their relative contributions, we entered these two variables into a multiple regression model (with every unit as one observation), predicting SUA PPC, separately for each attention condition. We show the difference in regression T-statistics between attention conditions in Figures 7B and 7C. The effect described above for the overall sustained firing rates held for both the baseline rate (BS and NS, $p < 0.01$ and $p < 0.05$ respectively, bootstrap test) and the rate change relative to baseline (BS and NS, $p < 0.01$ and $p < 0.05$ respectively, bootstrap test). The effect was again specific for the gamma-frequency band. In fact, a unit's baseline firing rate (NS: T-stat = 2.71, $p < 0.01$; BS: 3.51, $p < 0.001$) positively predicted its gamma PPC when selective attention was directed inside its RF, but not when it was directed outside its RF (NS: −0.39; BS: −0.15, all n.s.). Similarly, a BS cell's firing rate change relative to baseline (NS: T-stat = 1.59, n.s.; BS: 3.86, $p < 0.01$) positively predicted its gamma PPC when selective attention was directed inside its RF, but not when it was directed outside its RF (NS: −0.9, n.s.; BS: 0.06, n.s.). Thus, neurons contributing more spikes to the population output tend to be more gamma locked when attention is directed inside, but not when it is directed outside their RF. This may result in enhanced MUA-LFP gamma locking with attention inside the RF, since a unit constitutes a greater proportion of the total MUA if it has a higher firing rate.

Thus, one or both of the above-mentioned scenarios likely holds true, i.e., high-rate SUAs might gamma lock disproportionally more with attention and/or strongly gamma locking SUAs might fire disproportionally more with attention. We aimed at investigating whether one of the two scenarios is more prominent. We first tested whether SUAs with high rates show more attentional enhancement of gamma locking. Across SUAs, the stimulus driven firing rate was positively correlated with the attentional effect on SUA-LFP locking [$PPC_{in} - PPC_{out}$], specifically in the gamma band (Figure 7D) (BS: Spearman $\rho = 0.44$, $p < 0.01$; NS: Spearman $\rho = 0.29$, n.s.; all cells: $\rho = 0.46$, $p < 0.001$, n = 62). Again, we investigated the effect of baseline and stimulus driven firing rates relative to baseline separately, through multiple regression analysis. Both, a cell's baseline firing rate (BS: T-stat = 2.86, $p < 0.05$; NS: T-stat = 2.42, $p < 0.05$; all cells: T-stat = 4.29, $p < 0.001$, n = 62) and baseline corrected firing rate (BS: T-stat = 1.91, $p < 0.1$; NS: T-stat = 0.87, n.s., n = 21; all cells: T-stat = 2.18, $p < 0.05$, n = 62), positively predicted the gamma PPC difference between the attention in and out condition [$PPC_{in} - PPC_{out}$] (Figures 7E and 7F). This effect was again confined to the gamma-frequency band. In agreement with these correlation analyses, a median split of firing rates across the population directly visualized the difference in the attentional effect on gamma locking of the cells. It was negative for the cells with low activity levels (Figure 7G) and positive for the cells with high activity levels (Figure 7H). Finally, we tested whether also the complementary scenario holds, namely that strongly gamma locking SUAs show more attentional rate enhancements. We found that NS cells that were more strongly gamma locking, had a higher attentional firing rate modulation [FR_{in}/FR_{out}] (Figure 7I; NS: Spearman $\rho = 0.47$, $p < 0.05$; BS: $\rho = 0.17$, n.s.).

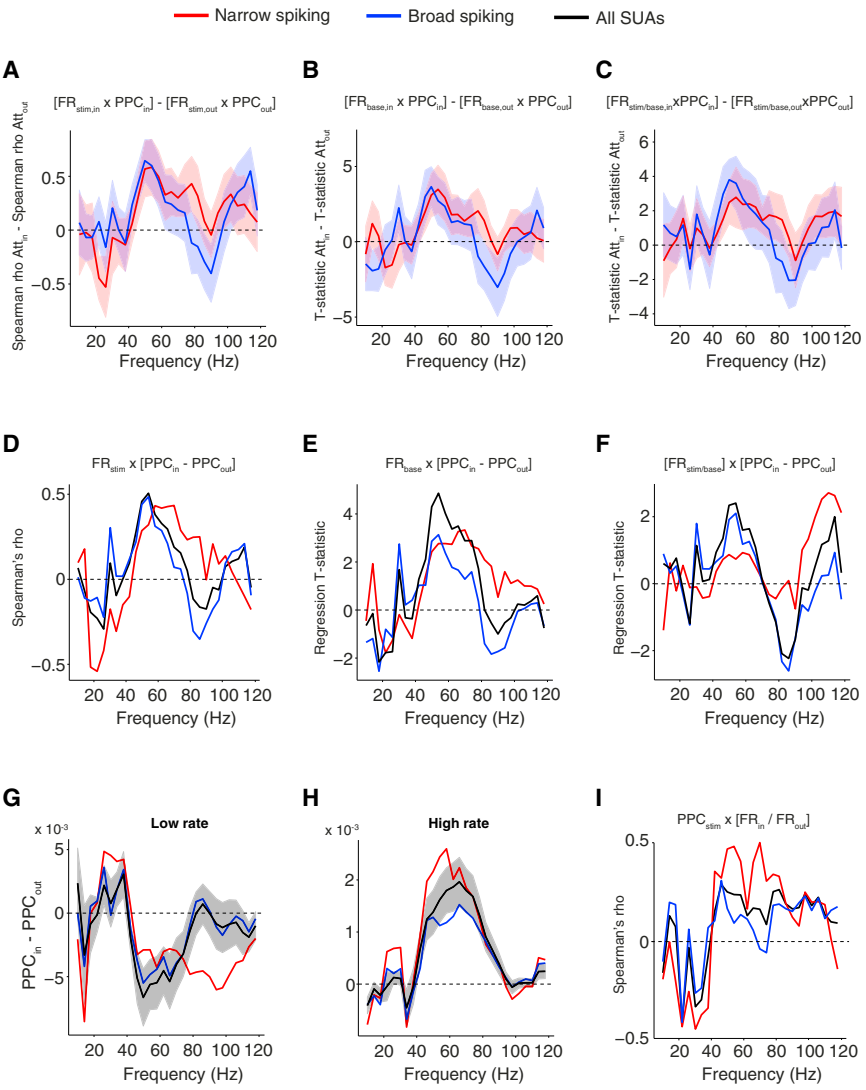

Figure 7. Relationships between PPC, Firing Rate, and Selective Attention

(A) Difference between attention conditions in Spearman correlations of PPC and stimulus period firing rate. Shadings indicate SEM.

(B) Same as (A), but now shown the difference between attention conditions in the T-statistic of the baseline firing rate predictor. This T-statistic was derived from a multiple regression of PPC onto baseline firing rate and relative stimulus firing rate to baseline.

(C) Same as (B), but now for the relative stimulus firing rate to baseline.

(D) Spearman correlation between stimulus driven firing rate and the attentional modulation of SUA PPC [$PPC_{in} - PPC_{out}$] versus frequency.

(E) Same as (D), but now shown the T-statistic of the baseline firing rate predictor.

(F) Same as (E), but now for relative stimulus firing rate to baseline.

(G and H) Average difference in PPC between attention conditions for units with low (G) and high (H) average firing rate (median split).

(I) Spearman correlation between PPC and attentional modulation of SUA firing rate [FR_{in}/FR_{out}] versus frequency.

See also Figures S1, S6, and S7.

DISCUSSION

This discussion is structured in three parts (1) the basic differences between NS and BS cell locking, (2) the diversity in locking phases, and (3) the effects of selective attention.

Basic Differences between NS and BS Cell Locking

We found that NS cells are almost twice as strongly locked to the LFP gamma rhythm as BS cells. The gamma locking of BS cells is essentially identical to the locking of MUA. To separate isolated single units into putative pyramidal cells and inhibitory interneurons, we used the same approach as many previous studies, clustering cells based on their AP waveforms (e.g., see Mitchell et al., 2007; Csicsvari et al., 1999). This approach does not provide absolute certainty about cell identity, but appears to be the best method available for the awake macaque monkey. In rodent preparations, optogenetic phototagging approaches can be used to identify the cell class with high precision (Cardin et al., 2009; Sohal et al., 2009). This optogenetic approach relies on genetically modified animals (Cre-Lox system) and is therefore not yet available for the monkey. Juxtacellular labeling followed by morphological reconstruction in rodents allows to identify only one or very few neurons per animal (e.g., Klausberger et al., 2003). While in the awake monkey, cell identity cannot be determined with similar precision, there is ample evidence supporting our interpretation of the NS and BS cell classes: (1) studies that identified cell identity unequivocally confirm the waveform separation used here (McCormick et al., 1985; Nowak et al., 2003; Hasenstaub et al., 2005; Gentet et al., 2010), (2) the distribution of waveform durations was clearly bimodal and contained a majority of BS cells, with observed proportions very close to those found in area V4 by Mitchell et al. (2007), and (3) firing rates were approximately twice as high for NS than BS cells, in good agreement with results obtained after unequivocal cell identification (McCormick et al., 1985; Connors and Gutnick, 1990; Contreras and Palmer, 2003; Gentet et al., 2010).

FS inhibitory interneurons, in particular the FS PV+ basket cell, are thought to be critically involved in the generation of gamma-band oscillations (Bartos et al., 2007; Buzsáki and Wang, 2012; Gulyás et al., 2010; Tiesinga and Sejnowski, 2009). To test whether FS PV+ cells play a causal role in the generation of gamma, Cardin et al. (2009) and Sohal et al. (2009) used optogenetic tools to control the firing of FS PV+ cells in vivo and found that exciting or inhibiting them increased or decreased gamma-band synchronization, respectively.

Our result that NS cells were approximately twice as strongly locked to the gamma rhythm as BS cells supports the idea that inhibitory interneurons play an important role in generating V4 gamma-band synchronization. So far, there has been little evidence from in vivo experiments for a predominant role of inhibitory interneurons in generating cortical gamma. van Wingerden et al. (2010) did not find stronger gamma locking for putative inhibitory interneurons as compared to putative pyramidal cells in awake rat orbitofrontal cortex. Hasenstaub et al. (2005) found approximately equally strong locking of RS and FS cells in anesthetized ferret prefrontal cortex (see their Figure 5), although membrane potential fluctuations in the gamma-band were more strongly conveyed by inhibitory postsynaptic potentials than excitatory postsynaptic potentials. Tukker et al. (2007) found that in the anesthetized rat CA1 area, FS basket cells were not particularly strongly gamma locked, while Csicsvari et al. (2003) found that in the awake rat CA1 and CA3 areas, a larger fraction of putative FS interneurons than putative pyramidal cells was significantly gamma locked.

An open question is to what degree the precise timing of pyramidal firing plays a role in generating gamma (Bartos et al., 2007; Buzsáki and Wang, 2012; Tiesinga and Sejnowski, 2009): The ING model has pyramidal cells simply entrained, while the PING model lends them a role in sustaining the rhythm after they are entrained. We have shown that during sustained visual activation, both NS and BS cells are entrained by the gamma rhythm, and BS cells fire before NS cells, as suggested by PING models (Börgers and Kopell, 2005; Eeckman and Freeman, 1990; Leung, 1982; Wilson and Cowan, 1972). This is consistent with previous findings showing that pyramidal cell activity has a gamma phase-lead of a few milliseconds over putative inhibitory interneuron activity (Csicsvari et al., 2003; Hasenstaub et al., 2005; Tukker et al., 2007; van Wingerden et al., 2010).

During the prestimulus cue period, we found that NS cells can lock to the gamma rhythm as strongly as during sustained activation, while BS cells show only marginal gamma entrainment. These observations suggest that gamma-rhythmic activity of inhibitory interneurons can be, to a large degree, uncoupled from the activity and gamma locking of local pyramidal cells. In turn, it also suggests that the strength of gamma in putative inhibitory interneurons is not necessarily inherited from gamma-rhythmic recurrent excitatory inputs. The observed dynamics during the prestimulus cue period were more consistent with an ING (Whittington et al., 1995; Wang and Buzsáki, 1996; Bartos et al., 2007) than a PING model.

The two different patterns of synchronization observed during the prestimulus cue period and the stimulus-driven activation might suggest a mixed model in which ING is implemented by top-down inputs, while PING is implemented by bottom-up stimulus drive. Under those conditions, ING might initially entrain PING, as it would limit the window of opportunity within which bottom-up inputs can drive the cells (Fries et al., 2001a)

Diversity in Locking Phases

We found that a given unit can be preferentially locking to essentially any phase in the gamma cycle and that this phase is largely the same during the fixation, cue, and stimulation period. Thus, the preferred gamma phase of firing appears largely to be a property of the cell, which could be related to (1) the particular cell subtype, (2) its position in the vertical cortical column, or (3) its position in the horizontal cortical map. We reported that, on average, BS cells fire ~60° before NS cells. Thus, cell type has some influence on the gamma phase of firing. Within these NS and BS cell classes, different cell subtypes might lock to different gamma phases, like in the case of hippocampal theta (Klausberger et al., 2003). This intriguing possibility requires future exploration, possibly utilizing optogenetic cell type identification strategies in the monkey. Yet, our data partly speak against this possibility, because the gamma phases of single units were more similar to the phases of the same-site MUA than to the phases of single units from other electrodes. This finding suggests that, besides the phase difference between pyramidal cells and inhibitory interneurons, local groups of neurons (as captured by a MUA recording) are locked to approximately the same phase of the gamma rhythm. This leaves a cell's position in the horizontal cortical map or vertical cortical column as the main candidate determinants of its preferred gamma phase. A position in the horizontal cortical map, during visual stimulation, translates to a particular position in the cortical activation map. A given stimulus typically generates an ordered spatial pattern of activation in the map, such that a cell's position in the map translates into a particular activation level. We have shown previously that the level of V1 activation further translates to the gamma phase (Vinck et al., 2010a). However, this effect accounted for only a relatively small part of the phase variance (see Figure 2 of Vinck et al., 2010a). The activation independent part of the phase variance (that is already visible in that figure and replicated here in Figure 4) likely requires a different explanation. We propose that it is related to the remaining possible source of phase variance, i.e., the position of a neuron in the vertical cortical column. In fact, there is direct evidence in favor of this suggestion: Livingstone (1996) has shown that pairs of gamma-synchronized neurons within the granular and supragranular layers of monkey V1 had the more superficial neuron lagging the deeper neuron by ~3 ms for a distance of ~400 μm. The dependence of gamma phase on the vertical position in the cortex might be due to the pattern of synaptic connections within a column and the resulting flow of activation. Gamma activity is primarily found in supragranular layers (Buffalo et al., 2011), and within those, the gamma phase of firing increases systematically with distance from the input layer 4 (Livingstone 1996). At the same time, a larger distance from layer 4 corresponds to a longer conduction time. Thus, the precise connectivity of the cortical column might generate the precise temporal sequence of gamma activation.

Therefore, we would like to suggest that a cell's preferred gamma phase is determined by two activation-independent factors (vertical position and cell class) and one activation-dependent factor (cf. gamma phase shifting). The interplay between these contributions to the gamma phase might explain the firing sequences and their stimulus dependence in anesthetized cat primary visual cortex (Havenith et al., 2011). The potential consequences of the different gamma-phase components are intriguing. First, the delay between pyramidal cell and interneuron spiking allows the gamma rhythm and in fact overall

activation to be maintained (Börgers and Kopell, 2005). If interneurons spike ahead of pyramidal cells, they would block network activity altogether (Kremkow et al., 2010). Second, the activation-dependent gamma phase shifts might play important roles in competition and/or spike-time dependent plasticity (Vinck et al., 2010a) Third, the vertical-position-dependent gamma phase might generate temporal input sequences that are optimal to activate postsynaptic neurons (Branco et al., 2010).

Effects of Selective Attention

For MUA-LFP gamma-band synchronization, we confirmed previous studies showing attentional enhancements in gamma-band LFP power and MUA-LFP coherence in awake monkey V4 (Fries et al., 2001b; Gregoriou et al., 2009). The importance of this confirmation derives from the methodological advance in that we demonstrate such enhancements for MUA-LFP gamma PPC, which is free of any bias due to spike count or spike rate. An open question addressed here is to what degree the effect of spatial attention on gamma locking is expressed in isolated single units and depends on electrophysiological cell class. Mitchell et al. (2007) showed that both putative interneurons and pyramidal cells have proportionally similar increases in firing rates with selective attention, a finding confirmed here. However, we found that SUA-LFP gamma-band PPC is reduced with attention across the population of BS cells and unaffected for NS cells when firing rate differences are not considered. We showed that the discrepancy between the attentional effect on SUA and MUA gamma locking can be explained by an interaction between the attentional effects on SUA firing rate and locking strength: Enhanced locking of strongly firing neurons might explain the discrepancy between MUA and SUA results given that a MUA's composition can change concordantly. We confirmed this by demonstrating that large attentional increases in gamma locking were seen for the most strongly firing SUs. When we performed a median split on SUA firing rate, the attentional effect on gamma-locking was negative for the weakly firing cells but positive for the strongly firing cells. It is conceivable that these particularly strongly firing/activated cells constitute a specific cell subclass.

These findings suggest that attention sharpens the composition of the synchronized assembly such that the most activated neurons are most synchronized and therefore exert the highest impact onto postsynaptic target neurons. Assuming that mainly the synchronized neurons effectively influence target neurons, a sharpening of the synchronized assembly potentially has an additional effect related to normalization mechanisms in the neuronal target group. Normalization mechanisms effectively lead to a situation in which different input neurons mutually reduce their respective gain. Therefore, eliminating less activated neurons from the synchronized assembly, and thereby from the postsynaptically effective assembly, might further enhance the relative gain of the more activated neurons.

EXPERIMENTAL PROCEDURES

Experiments followed guidelines of the National Institutes of Health with approval by the National Institute of Mental Health Intramural Animal Care and Use Committee. Monkeys performed a selective attention task. A trial started when the monkey touched a bar and directed its gaze within 0.7° of the fixation spot. After ~1.5 s, an attentional cue appeared. The cue was followed after ~0.75 s by two drifting grating stimuli, where one stimulus was cued as the target stimulus and one as the distractor stimulus. The monkey had to release the bar between 150 and 650 ms after a change in color of the target stimulus. The phase of each spike was determined by frequency decomposition of the LFP around each spike. We averaged the phases obtained from the LFPs recorded on all electrodes, except the electrode from which the spike was obtained. Up to four LFPs were recorded simultaneously. The strength of spike-LFP phase-locking was quantified by the PPC, which is unbiased by the number of spikes (Vinck et al., 2010a, 2012).

SUPPLEMENTAL INFORMATION

Supplemental Information includes Supplemental Experimental Procedures and seven figures and can be found with this article online at http://dx.doi.org/10.1016/j.neuron.2013.08.019.

ACKNOWLEDGMENTS

This work was supported by Human Frontier Science Program Organization grant RGP0070/2003 (P.F.), The Volkswagen Foundation Grant I/79876 (P.F.), the European Science Foundation European Young Investigator Award Program (P.F.), the European Union (HEALTH-F2-2008-200728 to P.F.), the LOEWE program ("Neuronale Koordination Forschungsschwerpunkt Frankfurt" to P.F.), the Smart Mix Programme of the Netherlands Ministry of Economic Affairs and the Netherlands Ministry of Education, Culture and Science (BrainGain to P.F.), The Netherlands Organization for Scientific Research grants 452-03-344 (P.F.) and 016-071-079 (T.W.), the National Institute of Mental Health Intramural Research Program (R.D.), and National Institutes of Health grant R01-EY017292 (R.D.). We thank J.H. Reynolds, A.E. Rorie, A.F. Rossi, and R.C. Saunders for help during the experiments.

Accepted: August 20, 2013
Published: November 20, 2013

REFERENCES

Barthó, P., Hirase, H., Monconduit, L., Zugaro, M., Harris, K.D., and Buzsáki, G. (2004). Characterization of neocortical principal cells and interneurons by network interactions and extracellular features. J. Neurophysiol. *92*, 600–608.

Bartos, M., Vida, I., and Jonas, P. (2007). Synaptic mechanisms of synchronized gamma oscillations in inhibitory interneuron networks. Nat. Rev. Neurosci. *8*, 45–56.

Bollimunta, A., Chen, Y., Schroeder, C.E., and Ding, M. (2008). Neuronal mechanisms of cortical alpha oscillations in awake-behaving macaques. J. Neurosci. *28*, 9976–9988.

Börgers, C., and Kopell, N. (2005). Effects of noisy drive on rhythms in networks of excitatory and inhibitory neurons. Neural Comput. *17*, 557–608.

Bosman, C.A., Schoffelen, J.M., Brunet, N., Oostenveld, R., Bastos, A.M., Womelsdorf, T., Rubehn, B., Stieglitz, T., De Weerd, P., and Fries, P. (2012). Attentional stimulus selection through selective synchronization between monkey visual areas. Neuron *75*, 875–888.

Branco, T., Clark, B.A., and Häusser, M. (2010). Dendritic discrimination of temporal input sequences in cortical neurons. Science *329*, 1671–1675.

Buffalo, E.A., Fries, P., Landman, R., Buschman, T.J., and Desimone, R. (2011). Laminar differences in gamma and alpha coherence in the ventral stream. Proc. Natl. Acad. Sci. USA *108*, 11262–11267.

Buschman, T.J., and Miller, E.K. (2007). Top-down versus bottom-up control of attention in the prefrontal and posterior parietal cortices. Science *315*, 1860–1862.

Buzsáki, G., and Wang, X.J. (2012). Mechanisms of gamma oscillations. Annu. Rev. Neurosci. *35*, 203–225.

Cardin, J.A., Carlén, M., Meletis, K., Knoblich, U., Zhang, F., Deisseroth, K., Tsai, L.-H., and Moore, C.I. (2009). Driving fast-spiking cells induces gamma rhythm and controls sensory responses. Nature *459*, 663–667.

Chalk, M., Herrero, J.L., Gieselmann, M.A., Delicato, L.S., Gotthardt, S., and Thiele, A. (2010). Attention reduces stimulus-driven gamma frequency oscillations and spike field coherence in V1. Neuron *66*, 114–125.

Cobb, S.R., Buhl, E.H., Halasy, K., Paulsen, O., and Somogyi, P. (1995). Synchronization of neuronal activity in hippocampus by individual GABAergic interneurons. Nature *378*, 75–78.

Connors, B.W., and Gutnick, M.J. (1990). Intrinsic firing patterns of diverse neocortical neurons. Trends Neurosci. *13*, 99–104.

Contreras, D., and Palmer, L. (2003). Response to contrast of electrophysiologically defined cell classes in primary visual cortex. J. Neurosci. *23*, 6936–6945.

Csicsvari, J., Hirase, H., Czurkó, A., Mamiya, A., and Buzsáki, G. (1999). Oscillatory coupling of hippocampal pyramidal cells and interneurons in the behaving Rat. J. Neurosci. *19*, 274–287.

Csicsvari, J., Jamieson, B., Wise, K.D., and Buzsáki, G. (2003). Mechanisms of gamma oscillations in the hippocampus of the behaving rat. Neuron *37*, 311–322.

Lopes da Silva, F.H., van Lierop, T.H., Schrijer, C.F., and van Leeuwen, W.S. (1973). Organization of thalamic and cortical alpha rhythms: spectra and coherences. Electroencephalogr. Clin. Neurophysiol. *35*, 627–639.

Eeckman, F.H., and Freeman, W.J. (1990). Correlations between unit firing and EEG in the rat olfactory system. Brain Res. *528*, 238–244.

Engel, A.K., Fries, P., and Singer, W. (2001). Dynamic predictions: oscillations and synchrony in top-down processing. Nat. Rev. Neurosci. *2*, 704–716.

Fries, P., Neuenschwander, S., Engel, A.K., Goebel, R., and Singer, W. (2001a). Rapid feature selective neuronal synchronization through correlated latency shifting. Nat. Neurosci. *4*, 194–200.

Fries, P., Reynolds, J.H., Rorie, A.E., and Desimone, R. (2001b). Modulation of oscillatory neuronal synchronization by selective visual attention. Science *291*, 1560–1563.

Fries, P., Womelsdorf, T., Oostenveld, R., and Desimone, R. (2008). The effects of visual stimulation and selective visual attention on rhythmic neuronal synchronization in macaque area V4. J. Neurosci. *28*, 4823–4835.

Gentet, L.J., Avermann, M., Matyas, F., Staiger, J.F., and Petersen, C.C. (2010). Membrane potential dynamics of GABAergic neurons in the barrel cortex of behaving mice. Neuron *65*, 422–435.

Gregoriou, G.G., Gotts, S.J., Zhou, H., and Desimone, R. (2009). High-frequency, long-range coupling between prefrontal and visual cortex during attention. Science *324*, 1207–1210.

Grothe, I., Neitzel, S.D., Mandon, S., and Kreiter, A.K. (2012). Switching neuronal inputs by differential modulations of gamma-band phase-coherence. J. Neurosci. *32*, 16172–16180.

Gulyás, A.I., Szabó, G.G., Ulbert, I., Holderith, N., Monyer, H., Erdélyi, F., Szabó, G., Freund, T.F., and Hájos, N. (2010). Parvalbumin-containing fast-spiking basket cells generate the field potential oscillations induced by cholinergic receptor activation in the hippocampus. J. Neurosci. *30*, 15134–15145.

Hasenstaub, A., Shu, Y., Haider, B., Kraushaar, U., Duque, A., and McCormick, D.A. (2005). Inhibitory postsynaptic potentials carry synchronized frequency information in active cortical networks. Neuron *47*, 423–435.

Havenith, M.N., Yu, S., Biederlack, J., Chen, N.H., Singer, W., and Nikolić, D. (2011). Synchrony makes neurons fire in sequence, and stimulus properties determine who is ahead. J. Neurosci. *31*, 8570–8584.

Henrie, J.A., and Shapley, R. (2005). LFP power spectra in V1 cortex: the graded effect of stimulus contrast. J. Neurophysiol. *94*, 479–490.

Klausberger, T., Magill, P.J., Márton, L.F., Roberts, J.D., Cobden, P.M., Buzsáki, G., and Somogyi, P. (2003). Brain-state- and cell-type-specific firing of hippocampal interneurons in vivo. Nature *421*, 844–848.

Kremkow, J., Aertsen, A., and Kumar, A. (2010). Gating of signal propagation in spiking neural networks by balanced and correlated excitation and inhibition. J. Neurosci. *30*, 15760–15768.

Leung, L.S. (1982). Nonlinear feedback model of neuronal populations in hippocampal CAI region. J. Neurophysiol. *47*, 845–868.

Livingstone, M.S. (1996). Oscillatory firing and interneuronal correlations in squirrel monkey striate cortex. J. Neurophysiol. *75*, 2467–2485.

Maris, E., Womelsdorf, T., Desimone, R., and Fries, P. (2013). Rhythmic neuronal synchronization in visual cortex entails spatial phase relation diversity that is modulated by stimulation and attention. Neuroimage *74*, 99–116.

McCormick, D.A., Connors, B.W., Lighthall, J.W., and Prince, D.A. (1985). Comparative electrophysiology of pyramidal and sparsely spiny stellate neurons of the neocortex. J. Neurophysiol. *54*, 782–806.

Mitchell, J.F., Sundberg, K.A., and Reynolds, J.H. (2007). Differential attention-dependent response modulation across cell classes in macaque visual area V4. Neuron *55*, 131–141.

Nolte, G., Ziehe, A., Nikulin, V.V., Schlögl, A., Krämer, N., Brismar, T., and Müller, K.R. (2008). Robustly estimating the flow direction of information in complex physical systems. Phys. Rev. Lett. *100*, 234101.

Nowak, L.G., Azouz, R., Sanchez-Vives, M.V., Gray, C.M., and McCormick, D.A. (2003). Electrophysiological classes of cat primary visual cortical neurons in vivo as revealed by quantitative analyses. J. Neurophysiol. *89*, 1541–1566.

Phillips, J.M., Vinck, M., Everling, S., and Womelsdorf, T. (2013). A long-range fronto-parietal 5- to 10-Hz network predicts "top-down" controlled guidance in a task-switch paradigm. Cereb. Cortex. http://dx.doi.org/10.1093/cercor/bht050.

Ray, S., and Maunsell, J.H.R. (2010). Differences in gamma frequencies across visual cortex restrict their possible use in computation. Neuron *67*, 885–896.

Shinomoto, S., Kim, H., Shimokawa, T., Matsuno, N., Funahashi, S., Shima, K., Fujita, I., Tamura, H., Doi, T., Kawano, K., et al. (2009). Relating neuronal firing patterns to functional differentiation of cerebral cortex. PLoS Comput. Biol. *5*, e1000433.

Sohal, V.S., Zhang, F., Yizhar, O., and Deisseroth, K. (2009). Parvalbumin neurons and gamma rhythms enhance cortical circuit performance. Nature *459*, 698–702.

Tiesinga, P., and Sejnowski, T.J. (2009). Cortical enlightenment: are attentional gamma oscillations driven by ING or PING? Neuron *63*, 727–732.

Tukker, J.J., Fuentealba, P., Hartwich, K., Somogyi, P., and Klausberger, T. (2007). Cell type-specific tuning of hippocampal interneuron firing during gamma oscillations in vivo. J. Neurosci. *27*, 8184–8189.

van Wingerden, M., Vinck, M., Lankelma, J.V., and Pennartz, C.M. (2010). Learning-associated gamma-band phase-locking of action-outcome selective neurons in orbitofrontal cortex. J. Neurosci. *30*, 10025–10038.

Vinck, M., Lima, B., Womelsdorf, T., Oostenveld, R., Singer, W., Neuenschwander, S., and Fries, P. (2010a). Gamma-phase shifting in awake monkey visual cortex. J. Neurosci. *30*, 1250–1257.

Vinck, M., van Wingerden, M., Womelsdorf, T., Fries, P., and Pennartz, C.M.A. (2010b). The pairwise phase consistency: a bias-free measure of rhythmic neuronal synchronization. Neuroimage *51*, 112–122.

Vinck, M., Battaglia, F.P., Womelsdorf, T., and Pennartz, C. (2012). Improved measures of phase-coupling between spikes and the Local Field Potential. J. Comput. Neurosci. *33*, 53–75.

Wang, X.J., and Buzsáki, G. (1996). Gamma oscillation by synaptic inhibition in a hippocampal interneuronal network model. J. Neurosci. *16*, 6402–6413.

Whittington, M.A., Traub, R.D., and Jefferys, J.G. (1995). Synchronized oscillations in interneuron networks driven by metabotropic glutamate receptor activation. Nature *373*, 612–615.

Wilson, H.R., and Cowan, J.D. (1972). Excitatory and inhibitory interactions in localized populations of model neurons. Biophys. J. *12*, 1–24.

Womelsdorf, T., Fries, P., Mitra, P.P., and Desimone, R. (2006). Gamma-band synchronization in visual cortex predicts speed of change detection. Nature *439*, 733–736.